Investigation of bone invasion and underlying mechanisms of oral cancer using a cell line-derived xenograft model

QIUSHENG SHAN[1,2], KIYOFUMI TAKABATAKE[1], HARUKA OMORI[1], HOTAKA KAWAI[1], MAY WATHONE OO[1], SHINTARO SUKEGAWA[1,3], MASAE FUJII[1], YASUNORI INADA[1], SHO SANO[1,2], KEISUKE NAKANO[1] and HITOSHI NAGATSUKA[1]

Departments of [1]Oral Pathology and Medicine and [2]Oral and Maxillofacial Surgery, Okayama University Graduate School of Medicine, Dentistry and Pharmaceutical Sciences, Okayama, Okayama 700-8525; [3]Department of Oral and Maxillofacial Surgery, Kagawa Prefectural Central Hospital, Takamatsu, Kagawa 760-8557, Japan

Received June 21, 2022; Accepted August 18, 2022

DOI: 10.3892/ol.2022.13502

Abstract. The cancer stroma regulates bone invasion in oral squamous cell carcinoma (OSCC). However, data on normal stroma are limited. In the present study, the effects of gingival and periodontal ligament tissue-derived stromal cells (G-SCs and P-SCs, respectively) and human dermal fibroblasts (HDFs) on bone resorption and osteoclast activation were assessed using hematoxylin and eosin and tartrate-resistant acid phosphatase staining in a cell line-derived xenograft model. The results demonstrated that G-SCs promoted bone invasion and osteoclast activation and inhibited osteoclast proliferation following crosstalk with the human OSCC HSC-3 cell line, whereas P-SCs inhibited bone resorption and promoted osteoclast proliferation *in vitro* but had a minimal effect on osteoclast activation both *in vitro* and *in vivo* following crosstalk with HSC-3 cells. Furthermore, the effects of G-SCs, P-SCs and HDFs on protein expression levels of matrix metalloproteinase (MMP)-9, membrane type 1 MMP (MT1-MMP), Snail, parathyroid hormone-related peptide (PTHrP) and receptor activator of NF-κB ligand (RANKL) in HSC-3 cells in OSCC bone invasion regions were assessed using immunohistochemistry. The results demonstrated that G-SCs had a more prominent effect on the expression of MMP-9, MT1-MMP, Snail, PTHrP, and RANKL, whereas P-SCs only promoted RANKL and PTHrP expression and exerted a minimal effect on MMP-9, MT1-MMP and Snail expression. The potential genes underlying the differential effects of G-SCs and P-SCs on bone invasion in OSCC were evaluated using a microarray, which indicated that cyclin-dependent kinase 1, insulin, aurora kinase A, cyclin B1 and DNA topoisomerase II alpha underlaid these differential effects. Therefore, these results demonstrated that G-SCs promoted bone invasion in OSCC by activating osteoclasts on the bone surface, whereas P-SCs exerted an inhibitory effect. These findings could indicate a potential regulatory mechanism for bone invasion in OSCC.

Correspondence to: Dr Kiyofumi Takabatake, Department of Oral Pathology and Medicine, Okayama University Graduate School of Medicine, Dentistry and Pharmaceutical Sciences, 2-5-1 Shikata-cho, Kita-ku, Okayama, Okayama 700-8525, Japan
E-mail: gmd422094@s.okayama-u.ac.jp

Key words: oral squamous cell carcinoma, bone invasion, gingival ligament tissue-derived stromal cell, periodontal ligament tissue-derived stromal cell, xenograft model, microarray

Introduction

Oral squamous cell carcinoma (OSCC), especially gingival OSCC (GOSCC), frequently invades the mandible or maxilla; jawbone destruction due to OSCC decreases the quality of life of patients (1-4). OSCC invades subgingival connective tissue, destroying the jawbone via vertical infiltration or reaching the periodontal ligament (PDL) tissue via horizontal infiltration. OSCC induces osteoclasts that produce bone resorption in and around cancerous tissue, destroying the jawbone as they progress deeper into the jaw (5). The nature of OSCC bone destruction is hypothesized to be a result of differential activation of osteoclasts by cancer cells, but the mechanism is unknown. To date, several studies have reported mechanisms of bone resorption in OSCC, which were relevant with the size of OSCC and the expression level of osteoprotegerin (3,4). However, the complete picture of bone resorption in OSCC is not yet clear. Multiple animal models are available for the study of OSCC bone resorption (6). Histologically, bone destruction by OSCC is directly mediated by osteoclasts rather than by cancer cells (7,8); In bone invasion of OSCC, osteoclastogenesis is mediated by receptor activator of nuclear factor κB (RANK), RANK ligand (RANKL) and osteoprotegerin, which belong to the tumor necrosis factor (TNF) family (9-12). OSCC cells promote expression of RANKL in stromal cells (SCs) and osteoclasts near OSCC bone invasion regions by secreting factors such as parathyroid hormone-related peptide (PTHrP), interleukin (IL)-6, IL-11, TNF-α and prostaglandin E2 (13-16). Furthermore, SCs in the tumor microenvironment of OSCC secret IL-6 to promote RANKL production in fibroblastic SCs (17). Therefore, it is necessary to study the

potential regulatory mechanisms of bone invasion to improve treatment and prognosis of patients with OSCC.

Solid tumors are composed of parenchymal and stromal components, which are hypothesized to regulate cancer progression by crosstalk with each other. In OSCC, an epithelial tumor, the interaction between the tumor parenchyma and stroma also serves a role in tumor progression (18,19). However, previous studies on the tumor stroma have only reported that the cancer parenchyma subordinately dominates the stroma and contributes to the progression of cancerous tissue (18,19); therefore, the mechanisms underlying the effect of the cancer stroma on the parenchyma are not clear. Our previous studies reported that the cancer stroma regulates bone invasion of human OSCC cell lines, HSC-2 and HSC-3 cells (20-23). Therefore, not only gingival cancer but also tongue cancer induces bone invasion. The behavior of OSCC is hypothesized to depend on its location; however, the mechanisms remain unknown (5). The tumor microenvironment of gingival epithelium-derived OSCC is complex and changes depending on direction of invasion (5). To the best of our knowledge, however, the effect of gingival-(G-) and PDL tissue-derived (P-)SCs in the GOSCC microenvironment on bone invasion in OSCC of different origins have been poorly investigated.

In the present study, the role of G-SCs and P-SCs in bone invasion in OSCC and their potential regulatory mechanisms were assessed. The differences in bone resorption capacity between gingival connective tissue and the PDL with respect to osteoclasts, MMPs and epithelial-mesenchymal transition (EMT) and RANKL and PTHrP, which have been reported as associated with bone resorption (22), were evaluated. The human OSCC HSC-3 cell line was selected for use as a cancer cell model as it is a moderately to poorly differentiated oral cancer cell line with bone invasion ability and is widely used in bone invasion studies (17,22). Similarly, the murine leukemia RAW264.7 cell line was selected for use as an osteoclast cell model based on its reported applications in bone invasion research (22,24). Human dermal fibroblasts (HDFs) were selected for use as a negative control for G-SCs and P-SCs as they are normal fibroblasts that remain unaffected by the cancer cells (23). The role and function of G-SCs and P-SCs in bone invasion of HSC-3 cells both *in vitro* and *in vivo* were evaluated. The present study will provide a potential regulatory mechanism for bone invasion in OSCC.

Materials and methods

Establishment of primary normal SCs. The human OSCC HSC-3 cell line (cat. no. JCRB0623), HDFs (cat. no. CC-2511) and the murine macrophage RAW264.7 cell line (cat. no. RCB0535) were purchased from the Japanese Collection of Research Bioresources Cell Bank, Lonza Group, Ltd. and RIKEN BioResource Center respectively. G-SCs and P-SCs were isolated from normal gingival tissue and the root surface of the tooth, respectively, of a male patient (age, 50 years), which were stored cells from the previous study (5). HSC-3 and RAW264.7 cells, G-SCs, P-SCs and HDFs were cultured in α-MEM (Thermo Fisher Scientific, Inc.) containing 10% fetal bovine serum (Biowest) and 1% antimycotic antibiotic (Thermo Fisher Scientific, Inc.) in a cell culture incubator at 37˚C in a humidified atmosphere of 5% CO_2. The present study was approved by the Ethics Committee of Okayama University (approval no. 1703-042-001). Written informed consent was obtained from the patient.

Tartrate-resistant acid phosphatase (TRAP) staining of cells. When cell density reached 90%, RAW264.7 and HSC-3 cells were collected using EDTA (Thermo Fisher Scientific, Inc.) and G-SCs, P-SCs and HDFs were collected using Accutase® solution (Invitrogen; Thermo Fisher Scientific, Inc.) respectively. RAW264.7, G-SCs/P-SCs/HDFs and HSC-3 were mixed at a ratio of 3:3:1. The combined cells were added to a 6-well plate containing coverslips (22x22 mm) at a density of $3.5x10^5$ cells/well. After 3 days in the cell culture incubator (37˚C), the slides were washed three times with Tris-buffered saline (TBS) and fixed with 4% paraformaldehyde (PFA) for 15 min in room temperature. The slides were stained using a TRAP staining kit (cat. no. AK04F; Cosmo Bio Co., Ltd.) in a 37˚C incubator overnight after washing three times with TBS. The percentage of positive osteoclast cells (defined as the percentage of TRAP-positive cells) and proliferation of osteoclast cells were calculated from ten images acquired using a BX51 bright-field microscope (magnification, x40; Olympus Corporation) and ImageJ software (version 1.53; National Institutes of Health). Independent experiments were performed three times.

Generation of HSC-3/SC xenograft mouse model. Animal research was performed in accordance with the guidelines and regulations (20) of the Animal Care and Use Committee, Okayama University (approval no. OKU-2022354). Anesthesia was performed as reported in Laboratory Animal Anesthesia, 3rd edition (ketamine hydrochloride, 75 mg/kg body weight; medetomidine hydrochloride, 0.5 mg/kg body weight) (25,26). Anesthetization of mice was confirmed by assessing whether mice returned to a prone position when placed on their backs. Following intraperitoneal anesthesia, 200 µl mixed cells (HSC-3, $1x10^6$, 100 µl mixed with G-SCs, P-SCs or HDFs, $3x10^6$, 100 µl) were injected into subcutaneous tissue on the top of the head of 20 healthy female BALB-nu-nu mice (age, 4 weeks; mean weight, 15 g; Shimizu Laboratory Supplies Co., Ltd.), as previously described (27). All mice were kept in the animal center of Okayama University, Okayama, Japan (25˚C; 50-60% humidity; 12/12-h light/dark cycle) and had free access to food and water. The health and behavior of mice were assessed by daily. The animals were kept for 4 weeks after cancer cell transplantation. If the transplanted tumor reached ≥10 mm in diameter or animals exhibited weight loss ≥20% over a 3-day period or decreased food and water intake or motility, the experiment was terminated immediately and the animal was euthanized. The mice were divided into four groups (n=5) as follows: i) HSC-3; ii) HSC-3 + G-SCs; iii) HSC-3 + P-SCs and iv) HSC-3 + HDFs. The data from one mouse in each group with poor tumor formation were removed based on the size of tumor and the pathological diagnosis and the data from the remaining four mice in each group were retained for analysis.

Hematoxylin and eosin (H&E) staining. Mice were euthanized by excess inhalation of isoflurane (concentration >5%) after 4 weeks. Cardiac arrest was confirmed by pulse palpation prior

to cervical dislocation. The complete heads of the mice were collected, fixed with 4% PFA for 12 h in room temperature and soaked in 10% EDTA for 4 weeks at 4˚C. The samples were processed using paraffin wax and cut into 5 μm sections, which were used for H&E staining (Carrazi' hematoxylin, Muto Pure Chemicals Co., Ltd, 5 min and room temperature; eosin, Muto Pure Chemicals Co., Ltd, 7 min and room temperature) and imaged using a BX51 bright-field microscope (magnification, x40; Olympus Corporation).

TRAP staining of tissue. The 5-μm sections from each group were used for TRAP staining using a TRAP staining kit (cat. no. AK04F; Cosmo Bio Co., Ltd.) according to the aforementioned method. A total of five images of bone invasion regions were acquired using the bright-field microscope (magnification, x40) for TRAP-positive cell counts using ImageJ software.

Immunohistochemistry (IHC). The 5 μm thick sections from each group were subjected to antigen retrieval [microwave 1 or 8 min (350 W); 0.01 M tri-sodium citrate buffer (pH 6) and 0.01 M Dako Target Retrieval Solution (pH 9; cat. no. S2367; Agilent Technologies, Inc.)], blocked with 10% normal serum (Vector Laboratories) for 20 min at room temperature. Sections were incubated with primary antibodies as follows: Mouse anti-MMP-9 (1:20; cat. no. F-69; Kyowa Pharma Chemical Co., Ltd.), anti-membrane-type 1 MMP (MT1-MMP; 1:20; cat. no. F-86; Kyowa Pharma Chemical Co., Ltd.), anti-Snail + SLUG (1:200; cat. no. ab180714; Abcam), anti-RANKL (1:100; cat. no. bs-0747R; BIOSS) and anti-PTHrP (1:100, cat. no. 10817-1-AP; ProteinTech Group, Inc.) overnight at 4˚C. The secondary antibodies were avidin-biotin complexes from mouse (cat. no. PK-6102) and rabbit (cat. no. PK-6101) ABC kit; Blocking serum (normal serum, diluted with TBS, at 1:75); biotinylated secondary antibody (diluted with normal serum, at 1:200); reagent A (avidin, ABC Elite, vector Laboratories, Inc.) and reagent B (biotinylated HRP, ABC Elite, Vector Laboratories, Inc., diluted with TBS, at 1:55) were added and incubated for 1 h at room temperature after washing with TBS three times and visualized using Histofine DAB substrate (Nichirei Biosciences, Inc.) at room temperature. A total of ten images (magnification, x40) of each mouse was acquired using a bright-field microscope to assess MMP-9, MT1-MMP, Snail, PTHrP and RANKL protein expression levels using IHC score by ImageJ software (version 1.53; National Institutes of Health). IHC scores were calculated as follows: IHC score=positive cell percentage score x intensity score. The positive cell percentage score was defined as follows: 0, <1; 1, 1-24; 2, 25-49; 3, 50-74 and 4, 75-100%. The intensity score was defined as follows: 0, negative; 1, weak (light yellow); 2, moderate (brown) and 3, strong staining (dark brown) (28). The staining results were assayed by two independent pathologists and and calculated as the mean value if the results were different between the two pathologists.

Bioinformatics analysis of microarray data. RNA was extracted from the cultured G-SCs and P-SCs by miRNeasy micro kit (Qiagen, Inc.) and quantified using NanoDrop One (NanoDrop; Thermo Fisher Scientific, Inc) and BioAnalyzerRNA6000 Nano (Agilent Technologies, In). cDNA synthesis, cRNA labeling and amplification were conducted using the Low Input Quick Amp Labeling Kit (Agilent Technologies, Inc.), and the purification of labeled cRNAs was conducted using RNeasy mini spin column (Qiagen, Inc.). Finally, the microarray (SurePrint G3 Human 8x60k ver.3.0; Agilent Technologies, Inc.) was scanned using a G4900DA Microarray Scanner (Agilent Technologies, Inc.). The differentially expressed genes (DEGs) in P-SCs compared with those in G-SCs were analyzed using GeneSpring GX14.9.1 (Agilent) with a cut-off value of LogFC >1 (ncbi.nlm.nih.gov/geo/query/acc.cgi?acc=GSE174595). Gene Ontology (GO) enrichment analysis was performed to define the biological process of upregulated (up)-DEGs in P-SCs using Cytoscape 3.7.2 (cytoscape.org/) with a cut-off value of adjusted P<0.05. The protein-protein interaction (PPI) network was produced to identify the hub genes using STRING (string-db.org/) and cytoHubba (version 0.1, cytoscape.org/apps/cytohubba) plugin for Cytoscape 3.7.2 with the cut-off value of combined score >0.4.

Statistical analysis. Statistical analysis was performed using GraphPad Prism 9 (GraphPad Software, Inc.). The cell experiments were repeated three times and the animal experiments were repeated in five independent mice. One-way ANOVA followed by Tukey's post hoc test was used for parametric data analysis (mean ± SD). Kruskal-Wallis followed by Dunn's test was used to analyze non-parametric data (median and interquartile range). P<0.05 was considered to indicate a statistically significant difference.

Results

G-SCs promote and P-SCs inhibit bone resorption. As both GOSCC and other origins of OSCC induce bone invasion or metastasis, the human OSCC HSC-3 cell line was selected as a model to assess the association between G-SCs/P-SCs and different origins of OSCC. The effects of G-SCs, P-SCs and HDFs on bone resorption of OSCC cells *in vivo* were assessed using H&E staining. The length of bone resorption in the HSC-3 + G-SCs group was markedly higher than that in the HSC-3, HSC-3 + HDFs groups and HSC-3+P-SCs groups. In addition, a notable keratinized area was observed in the HSC-3 + P-SCs group (Fig. 1A and B). Clinically, there are three types of bone invasion: Erosive, infiltrative and mixed. In erosive type of bone invasion, there is stroma between cancer cells and the bone. In infiltrative bone invasion, the cancer cells directly touch bone tissue without any stroma between them. Mixed bone invasion involves both erosive and infiltrative bone invasion (7). The remaining bone tissue of the HSC-3 and HSC-3 + G-SCs groups demonstrated erosive areas, which were bone resorption areas caused by cancer stroma and infiltrative areas that were directly resorbed by cancer cells. The HSC-3 + HDFs group also demonstrated both erosive and infiltrative areas; however, the bone resorption area was primarily within the erosive area. Moreover, the HSC-3 + P-SCs group demonstrated only erosive areas (Fig. 1C). Since these cell line-derived xenograft (CDX) models contained erosive and infiltrative areas, they demonstrated histological findings similar to those of actual human OSCC (7); therefore,

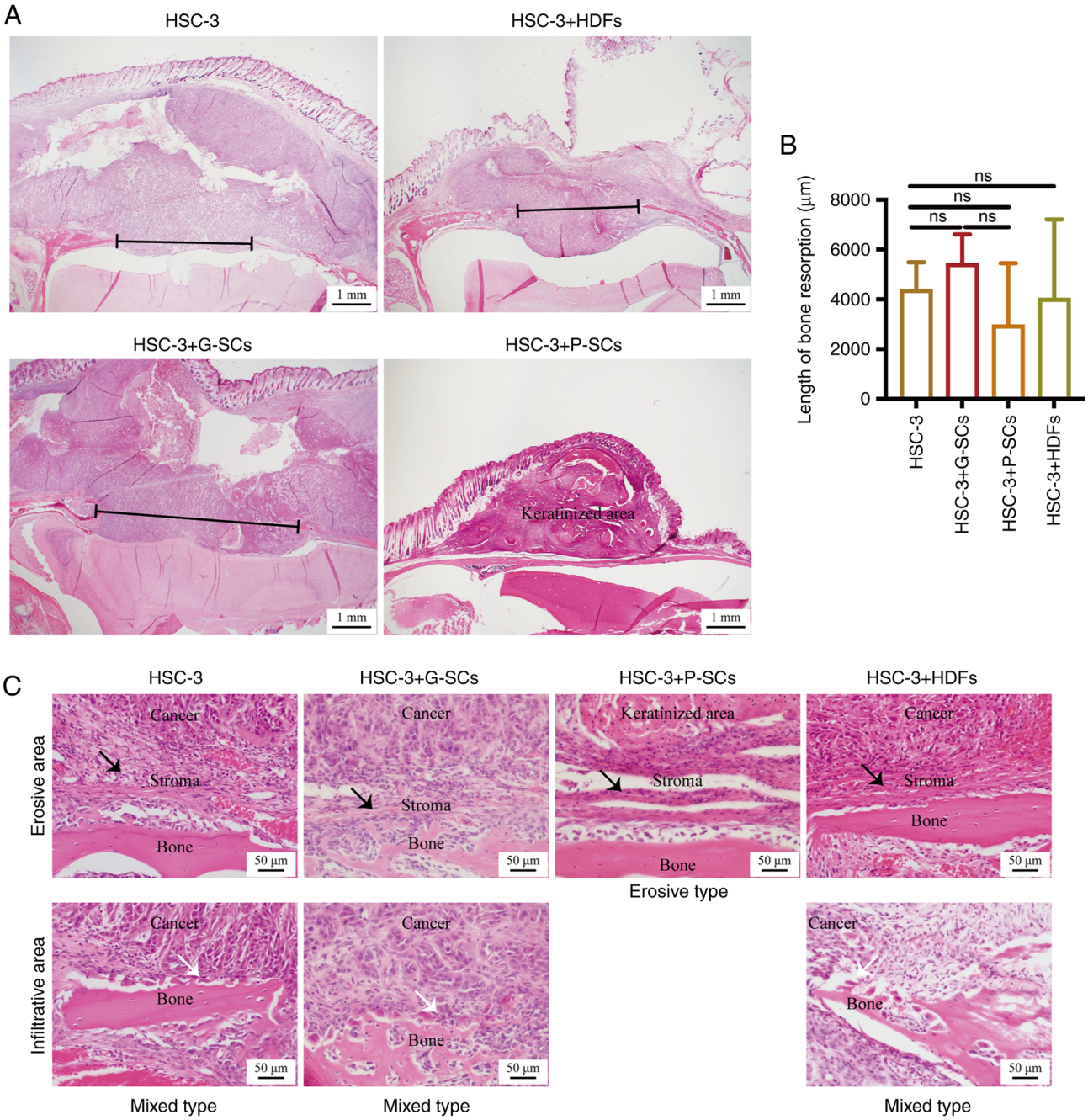

Figure 1. H&E staining to assess the effects of G-SCs, P-SCs and HDFs on bone invasion in OSCC *in vivo*. (A) H&E staining was used to assess bone mass. Black line, bone resorption. (B) Quantification of length of bone resorption. Data are presented as mean ± SD (n=4). Statistical analysis was performed using one-way ANOVA followed by Tukey's post hoc test. (C) H&E staining was used to assess the type of OSCC bone invasion. Black arrow, erosive area; white arrow, infiltrative area. H&E, hematoxylin and eosin; G-SCs, gingival tissue-derived stromal cells; P-SCs, periodontal ligament tissue-derived stromal cells; HDFs, human dermal fibroblasts; OSCC, oral squamous cell carcinoma; ns, not significant.

these CDX models were appropriate to mimic bone resorption in OSCC. Based on bone resorption length and invasion type, G-SCs exerted a promoting effect on bone invasion of OSCC, whereas P-SCs exerted an inhibitory effect and HDFs exerted a minimal effect.

G-SCs exert a more prominent promoting effect on invasion and EMT of HSC-3 in the erosive area of OSCC bone invasion region than P-SCs in vivo. IHC staining was used to assess MMP-9 and MT1-MMP protein expression levels to evaluate the effects of G-SCs, P-SCs and HDFs on invasion of HSC-3 cells in the OSCC bone invasion region (Fig. 2A and C). IHC scores of MMP-9 and MT1-MMP were significantly higher in the HSC-3 + G-SCs group compared with the HSC-3 and HSC-3 + P-SCs groups and there was little difference between the HSC-3, HSC-3 + P-SCs and HSC-3 + HDFs groups (Fig. 2B and D). Furthermore, osteoclasts on the bone surface were both MMP-9- and MT1-MMP-positive and the intensity of MMP-9 and MT1-MMP in the HSC-3 + G-SCs group was markedly higher than that in the other groups. IHC staining was used to assess Snail protein expression levels to evaluate the effects of G-SCs, P-SCs and HDFs on EMT of HSC-3 cells

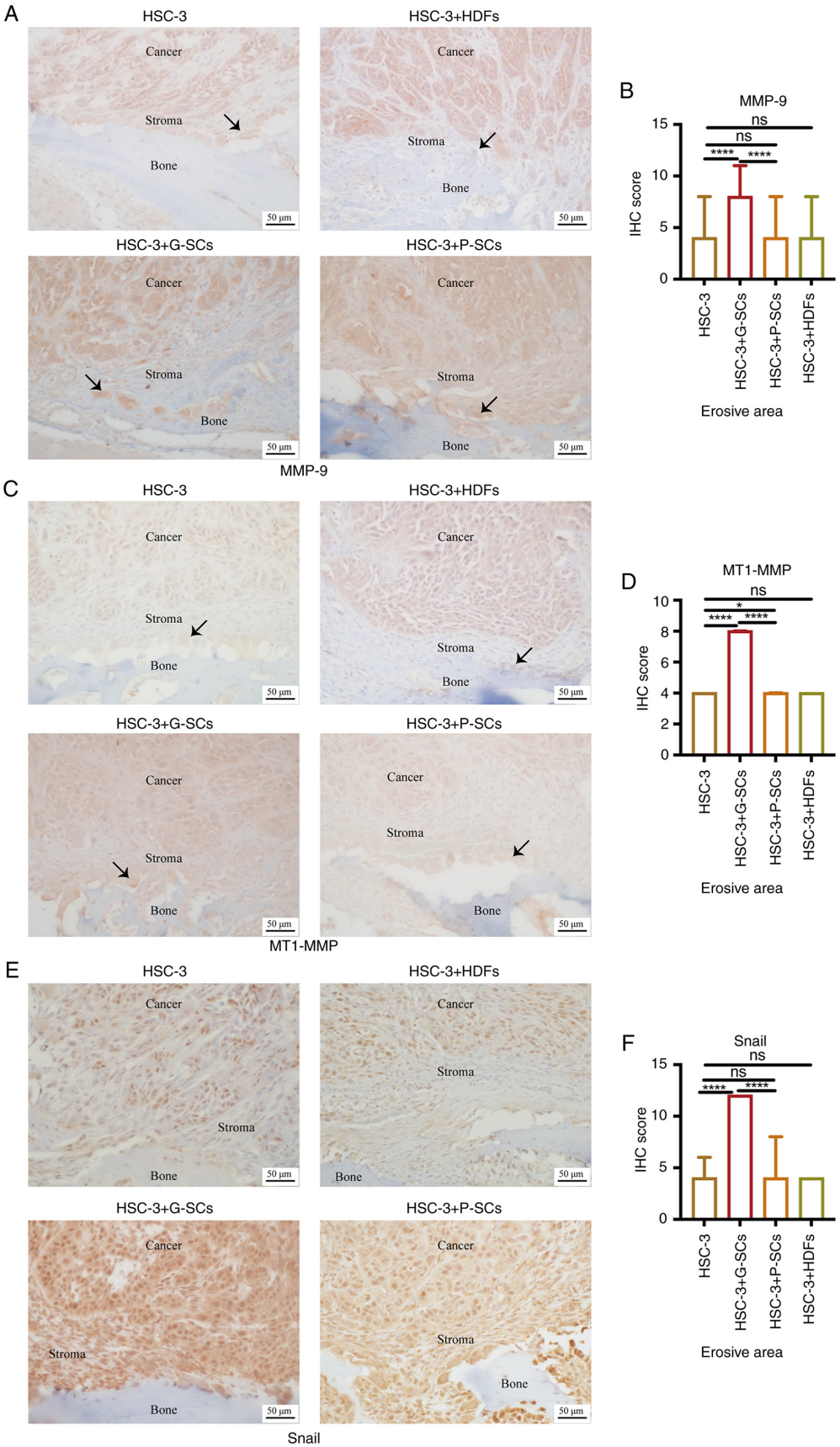

Figure 2. Effect of G-SCs, P-SCs and HDFs on invasion and EMT of HSC-3 cells in OSCC bone invasion region. Immunohistochemical staining was used to (A) assess and (B) quantify effect of G-SCs, P-SCs and HDFs on protein expression levels of MMP9. Immunohistochemical staining was used to (C) assess and (D) quantify effect of G-SCs, P-SCs and HDFs on protein expression levels of MT1-MMP. Immunohistochemical staining was used to (E) assess and (F) quantify effect of G-SCs, P-SCs and HDFs on protein expression levels of Snail. Black arrow, osteoclast. Data are presented as median and interquartile range (n=4). Statistical analysis was performed using Kruskal-Wallis followed by Dunn's test. *P<0.05 and ****P<0.0001. G-SCs, gingival tissue-derived stromal cells; P-SCs, periodontal ligament tissue-derived stromal cells; HDFs, human dermal fibroblasts; OSCC, oral squamous cell carcinoma; ns, not significant; EMT, epithelial-mesenchymal transition; MMP, matrix metalloproteinase; MT1-MMP, membrane type 1 MMP.

in the erosive area of OSCC bone invasion region (Fig. 2E). IHC score in the HSC-3 + G-SCs group was significantly higher compared with HSC-3 and HSC-3 + P-SCs groups but there was little difference between other groups (Fig. 2F). These results demonstrated that G-SCs promoted invasion and EMT of HSC-3 cells in the erosive area of the OSCC bone invasion region, whereas P-SCs and HDFs exerted a minimal effect.

Crosstalk between G-SCs and HSC-3 cells induces osteoclastogenesis more effectively than crosstalk between P-SCs and HSC-3 cells. TRAP staining was used to test the effects of G-SCs, P-SCs and HDFs on activation, differentiation and proliferationn of osteoclasts *in vitro*. There were only small round osteoclasts with a single nucleus in the RAW264.7 group as well as RAW264.7 cells with G-SCs and P-SCs (Fig. 3A). The percentage of TRAP-positive osteoclasts in the RAW264.7 group was significantly higher than in the RAW264.7 + HDFs, RAW264.7 + G-SCs and RAW264.7 + P-SCs groups. There was no significant difference between the RAW264.7 + G-SCs and RAW264.7 + P-SCs groups (Fig. 3C). The total number of osteoclasts was counted to assess the effects of G-SCs, P-SCs and HDFs on osteoclast proliferation *in vitro*. The total number of osteoclasts in the RAW264.7 + G-SCs and RAW264.7 + P-SCs groups was markedly higher than that in the RAW264.7 + HDFs group and significantly higher than that in the HSC-3 group. There was no significant difference between RAW264.7 + G-SCs and RAW264.7 + P-SCs groups (Fig. 3E). TRAP staining was used to assess the effects of G-SCs, P-SCs and HDFs on activation and cell proliferation of osteoclasts after crosstalk with HSC-3 cells *in vitro*. A previous study reported that differently shaped osteoclasts exert different effects on bone resorption; therefore, the shapes of osteoclasts in different groups were evaluated (29). The RAW264.7 + HSC-3, RAW264.7 + HSC-3 + P-SCs and RAW264.7 + HSC-3 + HDFs groups primarily presented round-shaped osteoclasts whereas the RAW264.7 + HSC-3 + G-SCs group presented round and triangular-shaped osteoclasts (Fig. 3B). The percentage of TRAP-positive osteoclasts in the RAW264.7 + HSC-3 + G-SCs group was significantly higher than that in the RAW264.7 + HSC-3 and RAW264.7 + HSC-3 + P-SCs groups and markedly higher than that in the RAW264.7 + HSC-3 + HDFs group. There was no significant difference between the RAW264.7 + HSC-3 and RAW264.7 + HSC-3 + P-SCs groups (Fig. 3D). The total number of osteoclasts in the RAW264.7 + HSC-3 + P-SCs group was significantly higher than that in the RAW264.7 + HSC-3 and RAW264.7 + HSC-3 + G-SCs groups and was markedly higher than that in the RAW264.7 + HSC-3 + HDFs group (Fig. 3F). TRAP-positive cells in the RAW264.7 + HSC-3, RAW264.7 + HSC-3 + G-SCs, RAW264.7 + HSC-3 + P-SCs, and RAW264.7 + HSC-3 + HDFs groups were markedly larger than those in RAW264.7, RAW264.7 + G-SCs, RAW264.7 + P-SCs and RAW264.7 + HDFs groups. TRAP staining was used to assess the proportion of activated osteoclasts on the bone surface to evaluate the effects of G-SCs, P-SCs and HDFs on osteoclast activation following crosstalk with HSC-3 *in vivo*. The HSC-3 group presented mainly round and ellipse-shaped osteoclasts on the bone surface. HSC-3 + P-SCs primarily presented ellipse-shaped osteoclasts and HSC-3 + HDFs mainly presented round and ellipse-shaped osteoclasts. The HSC-3 + G-SCs group presented round, ellipse and triangular osteoclasts (Fig. 3G). There was little difference in size of osteoclasts between groups (Fig. 3G). The number of TRAP-positive osteoclasts on the bone surface in the HSC-3 + G-SCs group was the highest, and there was no marked difference between the HSC-3, HSC-3 + P-SCs and HSC-3 + HDFs groups (Fig. 3H). Therefore, these data suggested that G-SCs, P-SCs and HDFs promoted cell proliferation and inhibited activation of osteoclasts and there was little difference between the effects of G-SCs and P-SCs. Following crosstalk with HSC-3 cells *in vitro*, G-SCs promoted activation and inhibited proliferation of osteoclasts, whereas P-SCs promoted proliferation of osteoclasts and exerted minimal effect on the activation of osteoclasts. HDFs exerted a minimal effect on activation and proliferation of osteoclasts following crosstalk with HSC-3 cells. These data suggested that crosstalk between HSC-3 cells and normal stroma may have increased size of activated osteoclasts *in vitro*. Moreover, the crosstalk between G-SCs and HSC-3 promoted activation of osteoclasts on the bone surface in the erosive area of the OSCC bone invasion region by regulating the shape and number of osteoclasts, whereas P-SCs and HDFs exerted a minimal effect *in vivo*.

G-SCs exert a more prominent promoting effect on RANKL and PTHrP protein expression levels in HSC-3 cells in the erosive area of OSCC bone invasion region than P-SCs. As RANKL regulates osteoclast activation (13), IHC staining was used to assess the effects of G-SCs, P-SCs and HDFs on RANKL protein expression levels in HSC-3 cells in the OSCC bone invasion region (Fig. 4A). IHC score in the HSC-3 + G-SCs group was markedly higher than that in the HSC-3 + HDFs group and significantly higher than in the HSC-3 and HSC-3 + P-SCs groups. There was no significant difference between the HSC-3 and HSC-3 + HDFs groups (Fig. 4B). As PTHrP not only recruits osteoclasts from peripheral blood but also regulates RANKL expression (30), IHC staining was used to assess the effects of G-SCs, P-SCs and HDFs on PTHrP protein expression levels in HSC-3 cells in the erosive area of OSCC bone invasion region (Fig. 4C). IHC score in the HSC-3 + G-SCs group was higher than that in the HSC-3 + P-SCs group and markedly higher than that in the HSC-3 and HSC-3 + HDFs groups. There was no significant difference between HSC-3 and HSC-3 + HDFs groups (Fig. 4D). These data demonstrated that both G-SCs and P-SCs promoted RANKL and PTHrP expression in HSC-3 cells in the OSCC bone invasion region. G-SCs exerted a significant promoting effect compared with P-SCs, whereas HDFs exerted no significant effect.

Cylin-dependent kinase 1 (CDK1), insulin (INS), aurora kinase A (AURKA), cyclin B1 (CCNB1) and DNA topoisomerase IIα (TOP2A) are potential genes underlying the differential effects of G-SCs and P-SCs on OSCC bone invasion following crosstalk with HSC-3 cells in vivo. The differential effects between G-SCs and P-SCs were evaluated using microarray analysis of DEGs. The biological processes of up-DEGs in P-SCs were analyzed by GO enrichment analysis, which indicated that these up-DEGs were primarily associated with biological processes such as ‘cell differentiation’, ‘cell migration’, ‘blood vessel development’ and ‘skeletal system

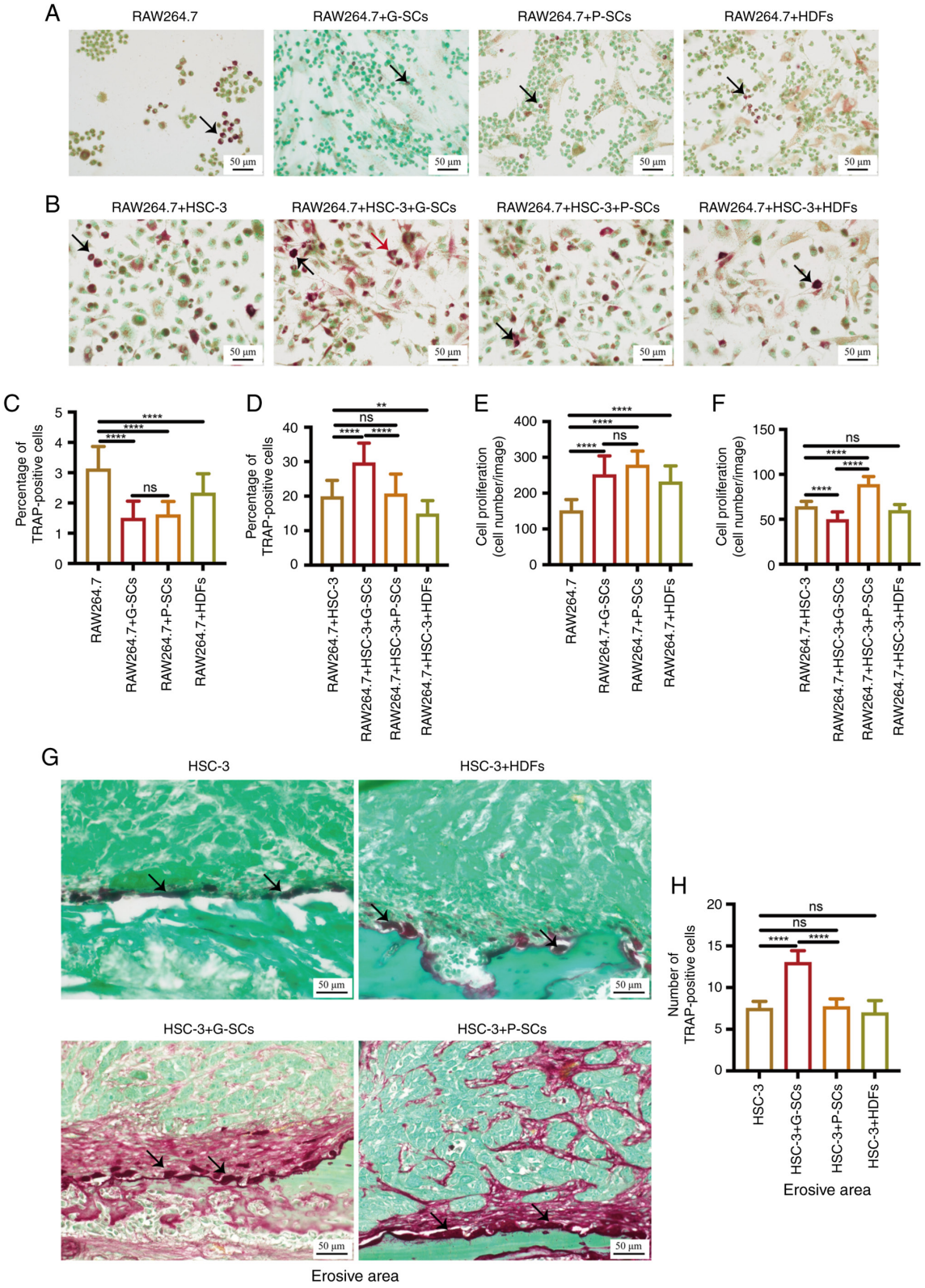

Figure 3. Effects of G-SCs, P-SCs and HDFs on activation of osteoclasts following crosstalk with HSC-3 cells both *in vitro* and *in vivo*. (A) TRAP staining was used to assess the effects of G-SCs, P-SCs and HDFs independently on activation and cell proliferation of osteoclasts *in vitro*. (B) TRAP staining was used to assess the effects of G-SCs, P-SCs and HDFs on activation and cell proliferation of osteoclasts following crosstalk with HSC-3 *in vitro*. Black arrow, round osteoclast; red arrow, triangular osteoclast. (C) Quantification of the percentage of TRAP-positive osteoclasts in RAW264.7, RAW264.7 + G-SCs, RAW264.7 + P-SCs and RAW264.7 + HDFs groups. (D) Quantification of the percentage of TRAP-positive osteoclasts in RAW264.7 + HSC-3, RAW264.7 + HSC-3 + G-SCs, RAW264.7 + HSC-3 + P-SCs and RAW264.7 + HSC-3 + HDFs groups. (E) Quantification of osteoclasts proliferation in RAW264.7, RAW264.7 + G-SCs, RAW264.7 + P-SCs, and RAW264.7 + HDFs groups. (F) Quantification of osteoclasts proliferation in RAW264.7 + HSC-3, RAW264.7 + HSC-3 + G-SCs, RAW264.7 + HSC-3 + P-SCs, and RAW264.7 + HSC-3 + HDFs groups. Data are presented as mean ± SD (n=3). (G) TRAP staining was used to assess the effects of G-SCs, P-SCs and HDFs on activation of osteoclasts on the bone surface following crosstalk with HSC-3 *in vivo*. Black arrow, activated osteoclast. (H) Quantification of TRAP-positive osteoclasts. Data are presented as mean ± SD (n=4). Statistical analysis was performed using one-way ANOVA followed by Tukey's post hoc test. **P<0.01 and ****P<0.0001. G-SCs, gingival tissue-derived stromal cells; P-SCs, periodontal ligament tissue-derived stromal cells; HDFs, human dermal fibroblasts; TRAP, tartrate-resistant acid phosphatase; ns, not significant.

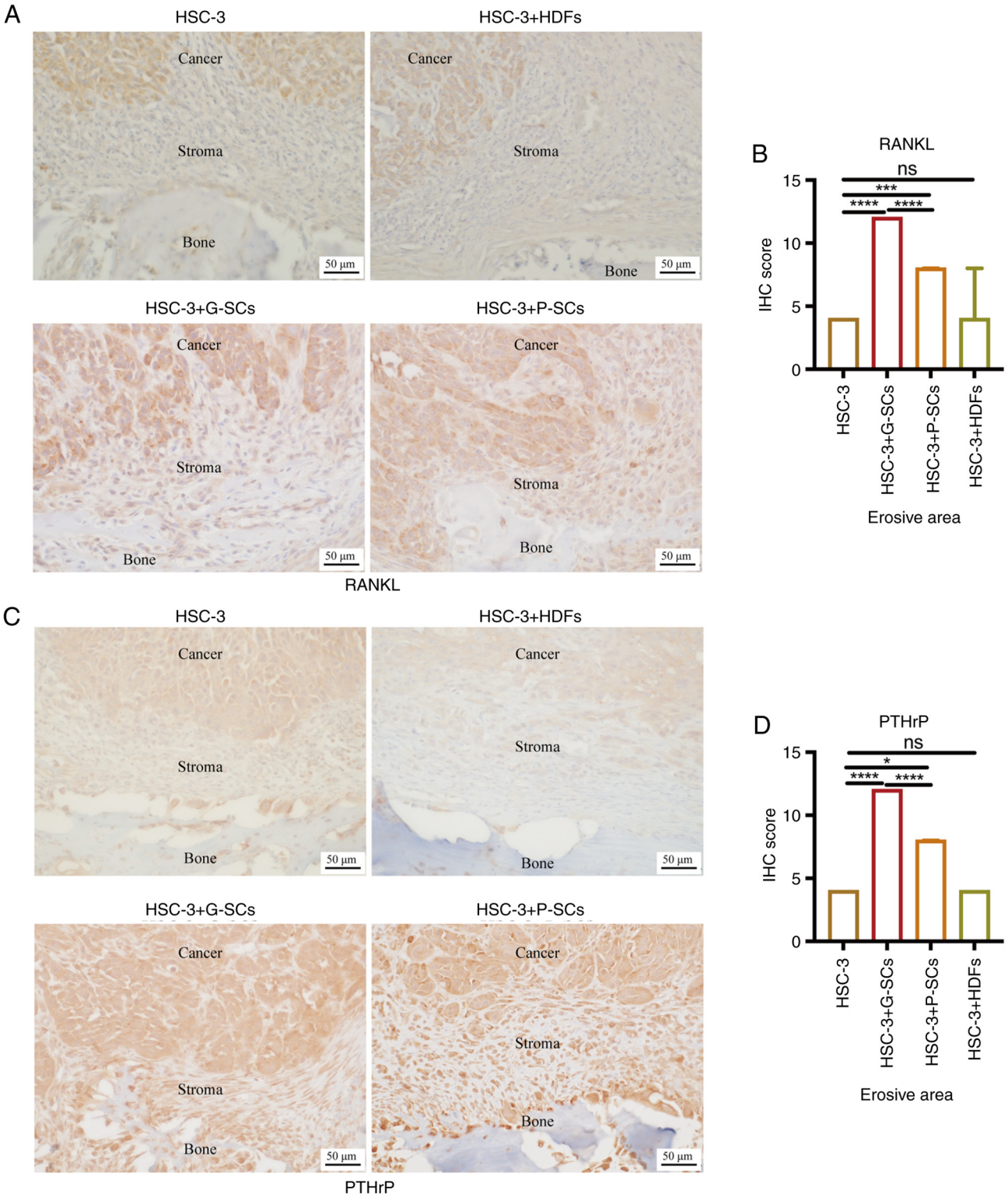

Figure 4. Effects of G-SCs, P-SCs and HDFs on the protein expression levels of RANKL and PTHrP in HSC-3 cells in the erosive area of OSCC bone invasion region. Immunohistochemical staining was used to (A) assess and (B) quantify effect of G-SCs, P-SCs and HDFs on protein expression levels of RANKL. Immunohistochemical staining was used to (C) assess and (D) quantify effect of G-SCs, P-SCs and HDFs on protein expression levels PTHrP in HSC-3 cells in the erosive area of OSCC bone invasion region. Data are presented as median and interquartile range (n=4). Statistical analysis was performed by Kruskal-Wallis followed by Dunn's test. *P<0.05, ***P<0.001 and ****P<0.0001. IHC, immunohistochemistry; G-SCs, gingival tissue-derived stromal cells; P-SC, periodontal ligament tissue-derived stromal cell; HDFs, human dermal fibroblasts; OSCC, oral squamous cell carcinoma; ns, not significant.

development', which are associated with bone invasion (Fig. 5A). The degree of differentiation leads to differential effects of G-SCs and P-SCs on OSCC bone invasion following crosstalk with HSC-3 cells *in vivo* and 'cell differentiation' was the most relevant biological process. Furthermore, hub genes in 'cell differentiation' were identified using the PPI network; *CDK1*, nucleolar and spindle associated protein 1 (*NUSAP1*), centromere protein F (*CENPF*), assembly factor

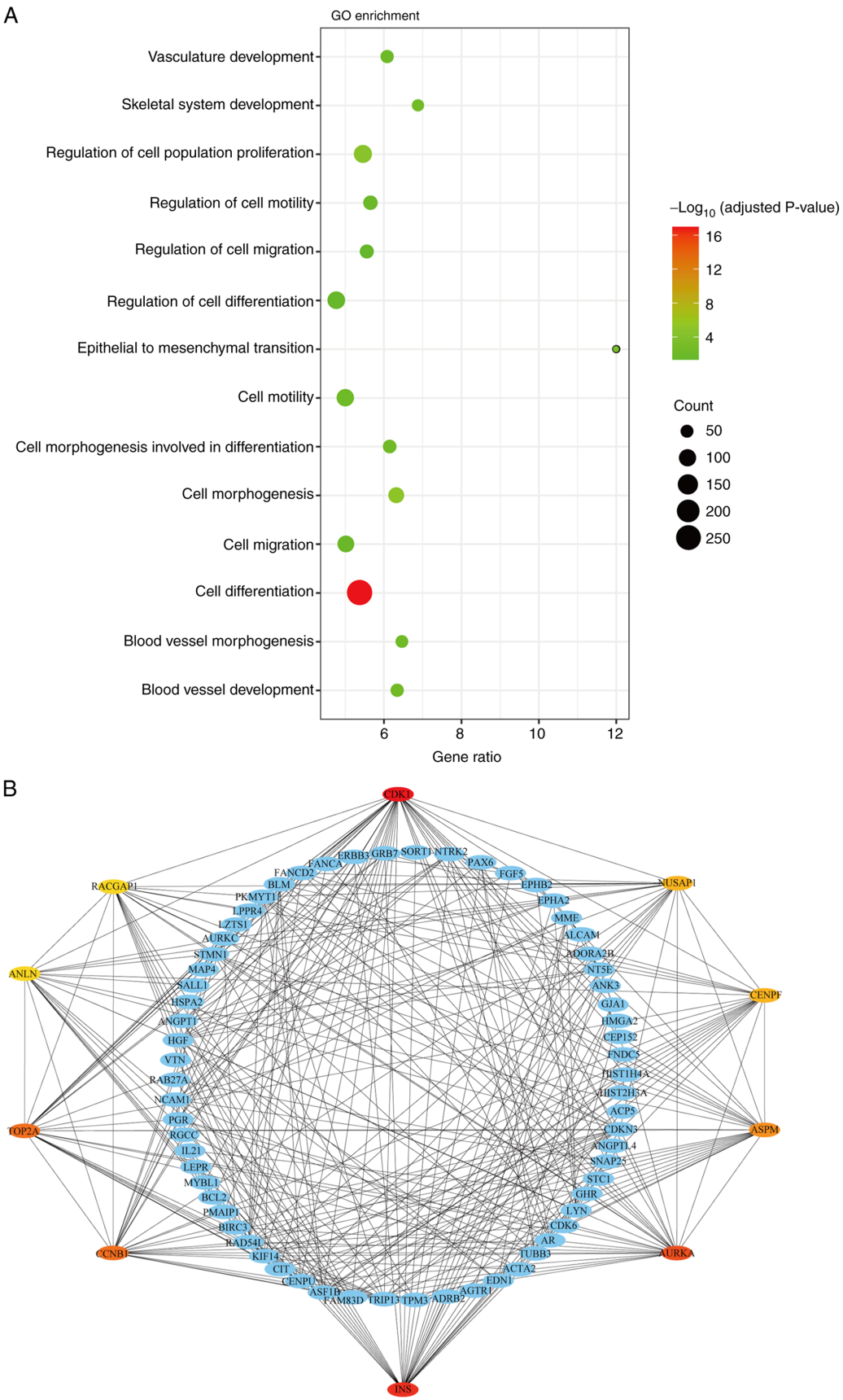

Figure 5. Identification of potential genes underlying the differential effects of G-SCs and P-SCs on OSCC bone invasion following crosstalk with HSC-3 cells *in vivo*. (A) Biological processes associated with upregulated differentially expressed genes in P-SCs was assess using Gene Ontology enrichment analysis (only presenting the potential biological process underlying the differential effects of G-SCs and P-SCs on OSCC bone invasion following crosstalk with HSC-3 *in vivo*). (B) Protein-protein interaction network was used to identify the hub genes in biological process of 'cell differentiation'. G-SC, gingival tissue-derived stromal cells; P-SCs, periodontal ligament tissue-derived stromal cells; OSCC, oral squamous cell carcinoma; CDK1, cylin-dependent kinase 1; INS, insulin; AURKA, aurora kinase A; CCNB1, cyclin B1; TOP2A, DNA topoisomerase IIα; NUSAP1, nucleolar and spindle-associated protein 1; CENPF, centromere protein F; ASPM, assembly factor for spindle microtubules; ANLN, anillin actin binding protein; RACGAP1, Rac GTPase activating protein 1.

for spindle microtubules (*ASPM*), *AURKA*, *INS*, *CCNB1*, *TOP2A*, anillin actin binding protein (*ANLN*) and Rac GTPase activating protein 1 (*RACGAP1*) were the top 10 hub genes involved in cell differentiation (Fig. 5B). As demonstrated by coloration of the hub genes, *CDK1*, *INS*, *AURKA*, *CCNB1* and *TOP2A* were more relevant to 'cell differentiation', which suggested that they may underlie the different effects of G-SCs and P-SCs on OSCC bone invasion following crosstalk with HSC-3 cells.

Discussion

The results of the present study suggested that both G-SCs and P-SCs exerted differential effects on the bone invasion of OSCC, which may cause by their differential effects on the differentiation degree of OSCC. *CDK1*, *INS*, *AURKA*, *CCNB1* and *TOP2A* have much potential to underlie this differential effect on the differentiation degree of OSCC. However, the effect of G-SCs and P-SCs on the bone invasion of OSCC need to be examined on the other types of oral cancer cell lines and the detail function of different size and shape of osteoclasts in the OSCC bone invasion need to be further studied. Finally, the detail role and function of *CDK1*, *INS*, *AURKA*, *CCNB1* and *TOP2A* in G-SCs and P-SCs on bone invasion of OSCC need to be further investigated.

Epithelial tumors influence neighboring normal stroma and utilize it for tumor tissue extension (5). However, the effects of different properties of the normal stroma on bone resorption have not yet been fully elucidated. Our previous studies assessed the effect of different subtypes of cancer stroma on bone invasion of both HSC-2 and HSC-3 cells (20-22). Furthermore, our previous study also assayed the effects of normal stroma G-SCs and P-SCs on bone invasion of OSCC but did not provide a detailed description of the bone invasion type and potential regulatory mechanism (5). In the present study, G-SCs and P-SCs were mixed with HSC-3 in a 3:1 ratio and were used to generate an animal model. Bone invasion of OSCC is classified into three types: Erosive, infiltrative and mixed (31,32). A previous study reported that the interaction between cancer-associated fibroblasts and cancer cells promoted bone invasion and prognosis of OSCC (27). The present study demonstrated that bone invasion of the HSC-3 + G-SCs group was of the mixed type, whereas the bone invasion of the HSC-3 + P-SCs group was erosive. This suggested that P-SCs induced change of bone invasion of HSC-3 cells from a mixed to erosive type. Based on degree of bone resorption, G-SCs promoted bone invasion, whereas P-SCs exerted an inhibitory effect. Furthermore, keratinized cancer cells were observed in the bone invasion region of the HSC-3 + P-SCs group. This type of cancer cell has low invasion and migration ability, which makes it difficult for them to approach the bone surface by EMT and results in bone invasion type changing from the mixed to erosive type (20). Moreover, HDFs in the present study were selected as controls; there was no significant difference between the HSC-3 and HSC-3 + HDFs groups. These results demonstrated that HDFs exerted a minimal effect on bone invasion of HSC-3 cells *in vivo*.

Bone invasion in OSCC is mediated by osteoclasts (33). A previous study generated animal models using the human tongue SCC SCC-25 cell line and reported different osteoclast shapes on the bone resorption surface (29). Our previous study demonstrated that the HSC-3 + squamous cell carcinoma-associated stromal cells (SCC-SCs) group contained triangular and round osteoclasts, whereas the HSC-3 + verrucous SCC-SCs group presented round, ellipse and triangular osteoclasts. In the present study, there were only round and ellipse-shaped osteoclasts in HSC-3 and HSC-3 + HDFs groups. Therefore, triangular osteoclasts demonstrated the best bone invasion ability, which indirectly confirmed the results of the aforementioned study (29). In the present study, RAW264.7 + G-SCs and RAW264.7 + P-SCs groups primarily presented round osteoclasts. Following crosstalk with HSC-3 cells *in vitro*, only the RAW264.7 + HSC-3 + G-SCs group demonstrated triangular osteoclasts and only round osteoclasts were observed in the other groups. Triangular osteoclasts were also demonstrated in the HSC-3 + G-SCs group *in vivo* and only round or ellipse-shaped osteoclasts were observed in the other groups. The crosstalk between G-SCs and HSC-3 cells promoted activation of osteoclasts and inhibited cell proliferation, whereas the crosstalk between P-SCs and HSC-3 cells promoted proliferation of osteoclasts and exerted a minimal effect on activation of osteoclasts. Crosstalk between HSC-3 cells and normal stroma exerted a more prominent promoting effect on the size of activated osteoclasts than the RAW264.7, RAW264.7 + G-SCs, RAW264.7 + P-SCs and RAW264.7 + HDFs groups *in vitro*. To the best of our knowledge, the present study is the first to demonstrate that normal stroma surrounding OSCC and experimental cancer stroma derived from OSCC induce similar responses in osteoblasts, which suggested that normal stroma may also serve a functional role in bone remodeling in OSCC. In the animal experiments, the number of activated osteoclast cells was significantly higher in the HSC-3 + G-SCs group and there was little difference between other groups. These data suggested that G-SCs promoted bone invasion of OSCC by regulating the shape, number and size of osteoclasts on the bone surface, whereas P-SCs exerted a minimal effect on the shape and number of osteoclasts on the bone surface. It has been previously reported that exposure to RANKL facilitates osteoclastogenesis in the murine macrophage cell line RAW264.7 (34). However, the association between OSCC bone invasion and osteoclasts from peripheral blood requires further investigation.

The bone invasion of OSCC is divided into initial, bone resorption and final phase (30). MMPs and EMT serve a key role in the bone invasion of OSCC. Cancer cells disrupt extracellular matrix by secreting MMPs and approach the bone surface via EMT (35-37). Our previous study suggested that cancer stroma promotes expression of MMP-9, MT1-MMP and Snail in HSC-3 cells in the OSCC bone invasion region (22). In the present study, G-SCs promoted MMP-9, MT1-MMP and Snail protein expression levels in HSC-3 cells in OSCC bone invasion regions, whereas P-SCs exerted a minimal effect. These data suggested that G-SCs caused promote cancer cells to approach the bone surface by secreting MMP-9 and MT1-MMP and, promoting EMT, whereas P-SCs exerted a minimal effect.

The bone resorption phase is mediated by activated osteoclasts (30). Osteoclast activation is regulated by colony-stimulating factor 1 and RANKL (38). A previous study reported that both oral cancer cells and cancer-associated

fibroblasts promote osteoclastogenesis by enhancing RANKL expression (39). Our previous study demonstrated that cancer stroma promotes RANKL expression in HSC-3 cells in OSCC bone invasion regions (22). In the present study, G-SCs and P-SCs promoted RANKL expression in HSC-3 cells in the OSCC bone invasion region, with G-SCs exerting a significantly greater effect than that exerted by P-SCs. PTHrP mediates RANKL expression (38) and recruitment of osteoclasts from circulating blood (30). In the present study, both G-SCs and P-SCs significantly promoted PTHrP expression in HSC-3 cells in OSCC bone invasion regions compared with HSC-3 cells, with G-SCs exerting a significantly greater effect than P-SCs. P-SCs exerted a minimal effect on the initial phase of the bone invasion based on the MMP9, MT1-MMP, and Snail expression; however, they had a promoting effect on bone resorption phase of bone invasion of OSCC based on the RANKL and PTHrP expression, which suggested that little bone invasion occurred in the HSC-3 + P-SCs group. These data suggested that P-SCs exerted an inhibitory effect on bone invasion of OSCC cells. Previous studies have also reported that PDL cells regulate bone resorption and formation by secreting cytokines (40,41). Here, however, P-SCs exerted an inhibitory effect on bone resorption in oral cancer, rather than a promoting effect, as observed in conditions such as inflammation and diabetes (42,43). Therefore, it can be hypothesized that bone invasion in OSCC was primarily caused by cancer rather than PDL cells and P-SCs indirectly affected OSCC bone invasion by interacting with cancer cells instead of directly regulating bone resorption.

The effects of G-SCs and P-SCs on bone invasion in OSCC were caused by effects on the degree of differentiation of HSC-3 cells in the OSCC bone invasion regions. P-SCs promoted differentiation of HSC-3 cells in the bone invasion regions, whereas G-SCs exerted an inhibitory effect. Therefore, G-SCs were used as the control group to assess DEGs in P-SCs using microarray analysis. The biological processes of up-DEGs in P-SCs were evaluated using GO enrichment analysis. The biological processes associated with differentiation, migration, vessel formation and bone development are considered to affect bone invasion in OSCC (22,23,30). Therefore, the biological processes were assessed and the most up-DEGs were enriched in 'cell differentiation'. PPI was used to identify hub genes involved in 'cell differentiation', which indicated that *CDK1*, *NUSAP1*, *CENPF*, *ASPM*, *AURKA*, *INS*, *CCNB1*, *TOP2A*, *ANLN* and *RACGAP1* were the top 10 hub genes. *CDK1*, *INS*, *AURKA*, *CCNB1* and *TOP2A* were most relevant to cell differentiation.

In conclusion, G-SCs promoted bone invasion in OSCC, whereas P-SCs exerted an inhibitory effect. The differential effects of G-SCs and P-SCs on bone invasion in OSCC were assessed using differentiation of HSC-3 cells in OSCC bone invasion regions. *CDK1*, *INS*, *AURKA*, *CCNB1* and *TOP2A* were potential genes that underlie the differential effects on differentiation of HSC-3 cells in OSCC bone invasion regions. To the best of our knowledge, the present study is the first to provide *in vivo* and *in vitro* evidence that normal stromal characteristics serve a key role in bone invasion in OSCC. The present data suggested that the normal stroma may be promising as a novel therapeutic target for bone invasion. These findings may provide a potential regulatory mechanism for normal stroma regulation of bone invasion of OSCC.

Acknowledgements

Not applicable.

Funding

The present study was funded by the Japan Society for Promotion of Science KAKENHI Grants-in-Aid for Scientific Research (grant nos. JP20K10094, JP21K10043, JP21K17089, JP19K19159, JP20H03888 and JP22K10170).

Availability of data and materials

The datasets used and/or analyzed during the current study are available from the corresponding author on reasonable request. The microarray data generated in the present study can be found in the Gene Expression Omnibus under accession number GSE174595 or at ncbi.nlm.nih.gov/geo/query/acc.cgi?acc=GSE174595.

Authors' contributions

QS designed the study. QS, KT, HO, HK, MWO, YI, SSu, MF, SSa, KN and HN performed experiments and data analysis. QS and KT constructed figures. QS wrote the manuscript. KN and HN supervised the study and contributed to data interpretation and manuscript revision. KT and HN confirm the authenticity of all the raw data. All authors have read and approved the final manuscript.

Ethics approval and consent to participate

The present study was approved by the Ethics Committee of Okayama University (project identification code 1703-042-001). All animal experiments were performed in accordance with the relevant guidelines and regulations approved by the institutional committee of Okayama University (approval no. OKU-2022354).

Patient consent for publication

Not applicable.

Competing interests

The authors declare that they have no competing interests.

References

1. Warnakulasuriya S: Global epidemiology of oral and oropharyngeal cancer. Oral Oncol 45: 309-316, 2009.
2. Lee KC, Chuang SK, Philipone EM and Peters SM: Which clinicopathologic factors affect the prognosis of gingival squamous cell carcinoma: A population analysis of 4,345 cases. J Oral Maxillofac Surg 77: 986-993, 2019.
3. Kuk SK, Yoon HJ, Hong SD, Hong SP and Lee JI: Staging significance of bone invasion in small-sized (4cm or less) oral squamous cell carcinoma as defined by the American joint committee on cancer. Oral Oncol 55: 31-36, 2016.
4. Russmueller G, Moser D, Würger T, Wrba F, Christopoulos P, Kostakis G, Seemann R, Stadler V, Wimmer G, Kornek G, *et al*: Upregulation of osteoprotegerin expression correlates with bone invasion and predicts poor clinical outcome in oral cancer. Oral Oncol 51: 247-253, 2015.

5. Omori H, Shan Q, Takabatake K, Nakano K, Kawai H, Sukegawa S, Tsujigiwa H and Nagatsuka H: The origin of stroma influences the biological characteristics of oral squamous cell carcinoma. Cancers (Basel) 13: 3491, 2021.
6. Martin CK, Dirksen WP, Shu ST, Werbeck JL, Thudi NK, Yamaguchi M, Wolfe TD, Heller KN and Rosol TJ: Characterization of bone resorption in novel in vitro and in vivo models of oral squamous cell carcinoma. Oral Oncol 48: 491-499, 2012.
7. Wong RJ, Keel SB, Glynn RJ and Varvares MA: Histological pattern of mandibular invasion by oral squamous cell carcinoma. Laryngoscope 110: 65-72, 2000.
8. Ishikuro M, Sakamoto K, Kayamori K, Akashi T, Kanda H, Izumo T and Yamaguchi A: Significance of the fibrous stroma in bone invasion by human gingival squamous cell carcinomas. Bone 43: 621-627, 2008.
9. Teitelbaum SL and Ross FP: Genetic regulation of osteoclast development and function. Nat Rev Genet 4: 638-649, 2003.
10. Takayanagi H: Osteoimmunology: Shared mechanisms and crosstalk between the immune and bone systems. Nat Rev Immunol 7: 292-304, 2007.
11. Teitelbaum SL: Osteoclasts: What do they do and how do they do it? Am J Pathol 170: 427-435, 2007.
12. Suzuki T, Hayakawa T and Gomi K: GM-CSF stimulates mouse macrophages and causes inflammatory effects in vitro. J Hard Tissue Biol 28: 37-42, 2019.
13. Shibuya I, Takami M, Kawamoto M, Karakawa A, Nakamura S and Kamijo R: Immunohistochemical analysis of the distribution of RANKL-expressing cells and the expression of osteoclast-related markers in giant cell tumor of bone. J Hard Tissue Biol 29: 137-146, 2020.
14. Okamoto M, Hiura K, Ohe G, Ohba Y, Terai K, Oshikawa T, Furuichi S, Nishikawa H, Moriyama K, Yoshida H and Sato M: Mechanism for bone invasion of oral cancer cells mediated by interleukin-6 in vitro and in vivo. Cancer 89: 1966-1975, 2000.
15. Jimi E, Furuta H, Matsuo K, Tominaga K, Takahashi T and Nakanishi O: The cellular and molecular mechanisms of bone invasion by oral squamous cell carcinoma. Oral Dis 17: 462-468, 2011.
16. Ono K, Akatsu T, Kugai N, Pilbeam CC and Raisz LG: The effect of deletion of cyclooxygenase-2, prostaglandin receptor EP2, or EP4 in bone marrow cells on osteoclasts induced by mouse mammary cancer cell lines. Bone 33: 798-804, 2003.
17. Kayamori K, Sakamoto K, Nakashima T, Takayanagi H, Morita K, Omura K, Nguyen ST, Miki Y, Iimura T, Himeno A, *et al*: Roles of interleukin-6 and parathyroid hormone-related peptide in osteoclast formation associated with oral cancers: Significance of interleukin-6 synthesized by stromal cells in response to cancer cells. Am J Pathol 176: 968-980, 2010.
18. Valkenburg KC, de Groot AE and Pienta KJ: Targeting the tumour stroma to improve cancer therapy. Nat Rev Clin Oncol 15: 366-381, 2018.
19. Quail DF and Joyce JA: Microenvironmental regulation of tumor progression and metastasis. Nat Med 19: 1423-1437, 2013.
20. Takabatake K, Kawai H, Omori H, Qiusheng S, Oo MW, Sukegawa S, Nakano K, Tsujigiwa H and Nagatsuka H: Impact of the stroma on the biological characteristics of the parenchyma in oral squamous cell carcinoma. Int J Mol Sci 21: 7714, 2020.
21. Shan Q, Takabatake K, Omori H, Kawai H, Oo MW, Nakano K, Ibaragi S, Sasaki A and Nagatsuka H: Stromal cells in the tumor microenvironment promote the progression of oral squamous cell carcinoma. Int J Oncol 59: 72, 2021.
22. Shan Q, Takabatake K, Kawai H, Oo MW, Inada Y, Sukegawa S, Fushimi S, Nakano K and Nagatsuka H: Significance of cancer stroma for bone destruction in oral squamous cell carcinoma using different cancer stroma subtypes. Oncol Rep 47: 81, 2022.
23. Shan Q, Takabatake K, Kawai H, Oo MW, Sukegawa S, Fujii M, Nakano K and Nagatsuka H: Crosstalk between cancer and different cancer stroma subtypes promotes the infiltration of tumor-associated macrophages into the tumor microenvironment of oral squamous cell carcinoma. Int J Oncol 60: 78, 2022.
24. Quan J, Elhousiny M, Johnson NW and Gao J: Transforming growth factor-β1 treatment of oral cancer induces epithelial-mesenchymal transition and promotes bone invasion via enhanced activity of osteoclasts. Clin Exp Metastasis 30: 659-670, 2013.
25. Flecknell PA: Laboratory animal anesthesia. 3rd edition. Academic Press, San Diego, CA, 191-192, 2009.
26. Adams S and Pacharinsak C: Mouse anesthesia and analgesia. Curr Protoc Mouse Biol 5: 51-63, 2015.
27. An YZ, Cho E, Ling J and Zhang X: The axin2-snail axis promotes bone invasion by activating cancer-associated fibroblasts in oral squamous cell carcinoma. BMC Cancer 20: 987, 2020.
28. Chuang FH, Hsue SS, Wu CW and Chen YK: Immunohistochemical expression of RANKL, RANK, and OPG in human oral squamous cell carcinoma. J Oral Pathol Med 38: 753-758, 2009.
29. Quan J, Hou Y, Long W, Ye S and Wang Z: Characterization of different osteoclast phenotypes in the progression of bone invasion by oral squamous cell carcinoma. Oncol Rep 39: 1043-1051, 2018.
30. Quan J, Johnson NW, Zhou G, Parsons PG, Boyle GM and Gao J: Potential molecular targets for inhibiting bone invasion by oral squamous cell carcinoma: A review of mechanisms. Cancer Metastasis Rev 31: 209-219, 2012.
31. Brown JS, Lowe D, Kalavrezos N, D'Souza J, Magennis P and Woolgar J: Patterns of invasion and routes of tumor entry into the mandible by oral squamous cell carcinoma. Head Neck 24: 370-383, 2002.
32. Shaw RJ, Brown JS, Woolgar JA, Lowe D, Rogers SN and Vaughan ED: The influence of the pattern of mandibular invasion on recurrence and survival in oral squamous cell carcinoma. Head Neck 26: 861-869, 2004.
33. Ito M, Izumi N, Cheng J, Sakai H, Shingaki S, Nakajima T, Oda K and Saku T: Jaw bone remodeling at the invasion front of gingival squamous cell carcinomas. J Oral Pathol Med 32: 10-17, 2003.
34. Vincent C, Kogawa M, Findlay DM and Atkins GJ: The generation of osteoclasts from RAW 264.7 precursors in defined, serum-free conditions. J Bone Miner Metab 27: 114-119, 2009.
35. Kim H, Lee JH, Lee SK, Song NY, Son SH, Kim KR and Chung WY: Chemerin treatment inhibits the growth and bone invasion of breast cancer cells. Int J Mol Sci 21: 2871, 2020.
36. Woodward JK, Holen I, Coleman RE and Buttle DJ: The roles of proteolytic enzymes in the development of tumour-induced bone disease in breast and prostate cancer. Bone 41: 912-927, 2007.
37. van der Pluijm G: Epithelial plasticity, cancer stem cells and bone metastasis formation. Bone 48: 37-43, 2011.
38. Raggatt LJ and Partridge NC: Cellular and molecular mechanisms of bone remodeling. J Biol Chem 285: 25103-25108, 2010.
39. Elmusrati AA, Pilborough AE, Khurram SA and Lambert DW: Cancer-associated fibroblasts promote bone invasion in oral squamous cell carcinoma. Br J Cancer 117: 867-875, 2017.
40. Ueda M, Goto T, Kuroishi KN, Gunjigake KK, Ikeda E, Kataoka S, Nakatomi M, Toyono T, Seta Y and Kawamoto T: Asporin in compressed periodontal ligament cells inhibits bone formation. Arch Oral Biol 62: 86-92, 2016.
41. Nishigaki M, Yamamoto T, Ichioka H, Honjo KI, Yamamoto K, Oseko F, Kita M, Mazda O and Kanamura N: β-cryptoxanthin regulates bone resorption related-cytokine production in human periodontal ligament cells. Arch Oral Biol 58: 880-886, 2013.
42. Kats A, Gerasimcik N, Näreoja T, Nederberg J, Grenlöv S, Lagnöhed E, Desai S, Andersson G and Yucel-Lindberg T: Aminothiazoles inhibit osteoclastogenesis and PGE2 production in LPS-stimulated co-cultures of periodontal ligament and RAW 264.7 cells, and RANKL-mediated osteoclastogenesis and bone resorption in PBMCs. J Cell Mol Med 23: 1152-1163, 2019.
43. Liu R, Bal HS, Desta T, Krothapalli N, Alyassi M, Luan Q and Graves DT: Diabetes enhances periodontal bone loss through enhanced resorption and diminished bone formation. J Dent Res 85: 510-514, 2006.